*31st EPS Conference on Plasma Phys. London, 28 June - 2 July 2004 ECA Vol.**28G**, O-2.28 (2004)*

Influence of the Laser Prepulse on Proton Acceleration in Thin-Foil Experiments

M. Kaluza[1], J. Schreiber[1], J. J. Honrubia[2], M. I. K. Santala[1], G. D. Tsakiris[1], K. Eidmann[1], J. Meyer-ter-Vehn[1], and K.-J. Witte[1]

[1]*Max-Planck-Institut für Quantenoptik, Garching, Germany*
[2]*GIFI, Universidad Politecnica de Madrid, Spain*

Proton and ion acceleration using high-intensity lasers is a field of rapidly growing interest. For possible applications of proton beams produced in laser-solid interactions, the generation of beams with controllable parameters such as energy spectrum, brightness, and spatial profile is crucial. Hence, the physics underlying the acceleration processes has to be well understood. After the first proof-of-principle experiments [1, 2], systematical studies were carried out to examine the influence of target material and thickness [3, 4]. To establish the influence of the main laser parameters such as intensity, pulse energy, and duration over a wide range, results from different laser systems have to be compared, since usually each system covers a small parameter range only. Besides these parameters, strength and duration of the prepulse due to amplified spontaneous emission (ASE) play an important role, too [3]. The origin of the most energetic protons is still debated. There are at least two acceleration scenarios able to explain the occurance of MeV-protons. (i) They may come from the *front* surface of the target, i.e. the side irradiated by the laser pulse [1] or (ii) from the *rear* surface [2, 4]. Recent results indicate that both mechanisms act simultaneously [5], in accordance with the predictions of particle-in-cell (PIC) simulations [6, 7, 8].

We report on experiments carried out to establish the influence of the laser prepulse due to ASE and the target thickness on the acceleration of protons from thin aluminum foils. The protons originate from water and hydrocarbon contaminations on the foil surfaces. We used the 6-TW ATLAS laser facility at MPQ delivering 150 fs pulses at 790 nm wave length containing up to 900 mJ of energy. The pulses are focused by an $f/2.5$ off-axis parabolic mirror onto aluminum foils of $0.8 \ldots 86\,\mu$m thickness to intensities in excess of $10^{19}\,\mathrm{W/cm^2}$. The duration of the ASE prepulse having a peak intensity of $8 \times 10^{11}\,\mathrm{W/cm^2}$ can be controled by means of an ultra-fast Pockels cell in the laser chain. The shortest prepulse duration is 500 ps and it can be extended to several ns. The protons accelerated from the foils are detected by a Thomson parabola positioned in normal direction of the target rear side. CR 39 plates are used as a detector. The proton pits made visible by etching the CR 39 in NaOH after the shot are counted by an optical microscope equipped with a pattern-recognition software.

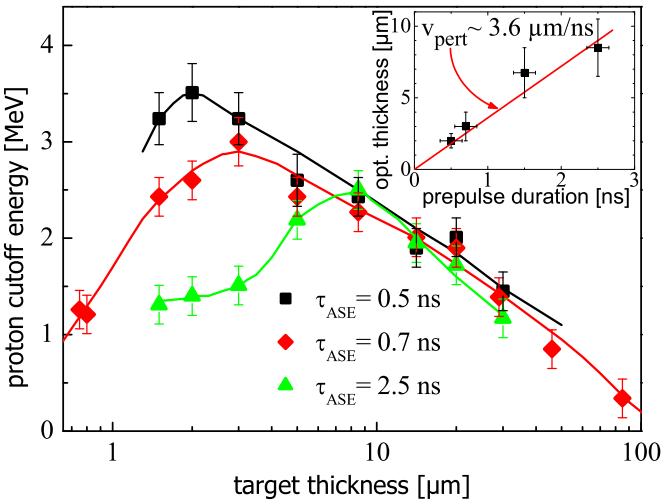

Figure 1: Proton cutoff energies for differently thick targets and prepulse durations, τ_{ASE}, of 0.5, 0.7 and 2.5 ns, respectively, at I_L=1.0 $\times$ 10^{19} W/cm^2. For longer τ_{ASE}, the maximum proton energies are achieved with thicker foils. The inset gives the optimal thickness, depending on τ_{ASE}.

We have performed several series of measurements, varying the ASE duration, τ_{ASE}, the laser intensity, I_L, and the target thickness. Fig. 1 shows the proton cutoff energies as measured with the Thomson parabola versus the target thickness for I_L=1.0 $\times$ 10^{19} W/cm^2 and ASE durations of 0.5, 0.7, and 2.5 ns, respectively. For each ASE duration we find that with increasing target thickness the cutoff energy first increases and then drops again. The highest proton energies are achieved at an optimal target thickness. When the prepulse duration is changed, this optimal value changes correspondingly, as it is shown in the inset. For thicker targets, the prepulse duration appears to have no effect on the proton cutoff energies, whereas for thinner targets and longer τ_{ASE} the cutoff energies are reduced [9]. When the peak laser intensity is slightly increased from 1.0 and 1.5 $\times$ 10^{19} W/cm^2, the peak proton energies increases as well, while the value for the optimal target thickness remains unaffected.

To study the influence of the ASE prepulse in more detail, we carried out 1-D simulations with the hydro-code MULTI-FS [10]. The intensity evolution of the prepulse was taken from the experiment. Fig. 2 shows the ion-density profiles of targets having different initial

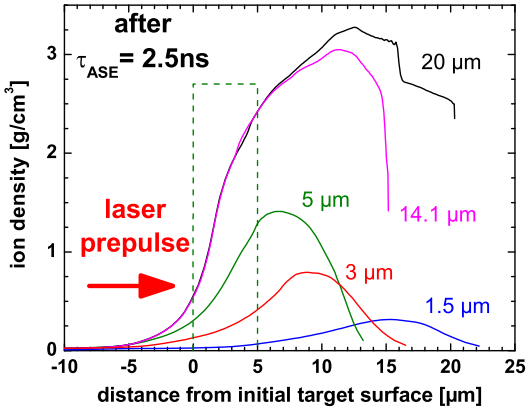

Figure 2: Ion-density profiles of targets having different initial thicknesses after 2.5 ns-irradiation by the ASE prepulse. The prepulse impinges from the left, the initial target front surface was situated at $x = 0\,\mu$m, as it is depicted for the 5 μm foil.

thicknesses after the irradiation by the prepulse just before the main pulse arrives on the tar-

get. Especially the thinnest foils have strongly expanded and the ion density is significantly reduced in these cases. For the thickest foils, the ion density remains high and also the target rear side remains unaffected. The propagation of the laser-generated MeV-electron pulse is described by a 2-D code for fast-electron transport (FET) [11]. The spatial and temporal shape of the electron pulse is determined by the laser-intensity distribution on the target front side. When these electrons propagate through the target density profiles, the background plasma is resistively heated by the return current, j_{return}, balancing the fast-electron current, j_{fast}. This spatially non-uniform heating leads to a spatial variation of the target conductivity, σ, that both depends on the target density, ρ, and temperature, T, and corresponds to a spatial variation of the electric field that further drives the return current. This finally leads to the formation of an azimuthal magnetic field that tends to pinch the electron beam as a whole. Note that the field generation depends on the background density and the temperature. A lower target density as present in expanded targets corresponds to a lower resistive heating, the generation of weaker electric and magnetic fields and therefore a less pronounced collimation of the electron beam. The FET code gives the mean densities, energies, and the pulse duration of the electrons exiting the target rear side for the different initial thicknesses. These values are then used to describe the rear-side proton acceleration by a 1-D code similar to [12], that further takes into account the effect of an initial ion-density gradient at the target rear side. Here, the proton acceleration is driven by the space-charge fields set up by the fast

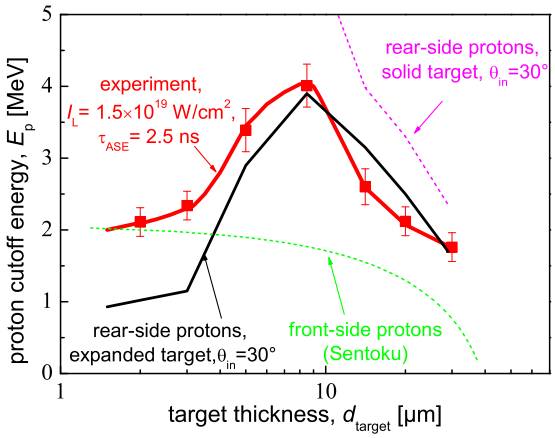

Figure 3: Comparison between experimentally measured proton cutoff energies with numerical results for rear-side acceleration including the electron transport (in solid or expanded targets) and predictions for the front-side acceleration.

electrons arriving at the rear side of the target. The effect of an prepulse-induced ion-density gradient, that was calculated by MULTI-FS, is also included in this code. The comparison of the numerically predicted peak proton energies with the experimental data is shown in Fig. 3. For targets thicker than 5 μm, the numerically predicted peak energies agree well with the experiment. Also the optimal target thickness, 8.5 μm for this prepulse duration, is well reproduced. For thicker targets, the simulations reveal that the electrons propagate through the

target in a well-collimated beam. Due to the resistive heating, the electrons loose a significant part of their energy. The proton acceleration fields that depend both on the electron density and mean energy at the target rear side [6] are reduced due to the energy loss, therefore the proton energies are reduced for increasing target thickness. The drop of proton energies towards thinner targets can be understood, as here the target has been strongly expanded and diluted due to the laser prepulse. The field generation inside the target is much weaker in this situation leading to a less collimated electron propagation and therefore to reduced rear-side electron densities, diminishing the proton acceleration fields. Additionally, these fields are reduced by the rear-side ion-density gradient only present for thin targets. For the thinnest targets, this leads to peak proton energies that are significantly lower than in the experiment. However, these measured proton energies can be well explained by the front-side acceleration process as described Sentoku *et al.* [8]. The peak energy of front-side accelerated protons is also given in Fig. 3, including the effect of proton stopping in the target.

In conclusion, we found that the peak-proton energies measured for different target thicknesses are only explainable taking into account both the rear-side acceleration mechanism that is influenced by the fast-electron transport inside the target and the front-side mechanism. At the optimal target thickness, the fastest protons come from the target rear side. For thinner targets, this mechanism is rendered ineffective by the prepulse-induced changes of the target properties. This reduces the peak proton energies below the value for the front-side accelerated protons.

References

1. A. Maksimchuk *et al.*, PRL **84**, 4108 (2000) and E. Clark *et al.*, PRL **84**, 670 (2000)
2. R. Snavely *et al.*, PRL **85**, 2945 (2000)
3. M. Roth *et al.*, Phys. Rev. STAB **5**, 061301 (2002)
4. A. Mackinnon *et al.*, PRL **86**, 1769 (2001) and PRL **88**, 215006 (2002)
5. M. Zepf *et al.*, PRL **90**, 064801 (2003) and S. Karsch *et al.*, PRL **91**, 015001 (2003)
6. S. Wilks *et al.*, Phys. Plasmas **8**, 542 (2001)
7. A. Pukhov, PRL **86**, 3562 (2001)
8. Y. Sentoku *et al.*, Phys. Plasmas **10**, 2009 (2003)
9. M. Kaluza *et al.*, accepted for publication in PRL (2004)
10. K. Eidmann *et al.*, PRE **62**, 1202 (2000)
11. J. J. Honrubia *et al.*, accepted for publication in Las. Part. Beams (2003)
12. J. Crow *et al.*, Phys. Fluids **14**, 65 (1975)